Journal of Manufacturing Science and Engineering. Received February 11, 2021;
Accepted manuscript posted May 10, 2021. doi:10.1115/1.4051189

Finite Element Model of Equal Channel Angular Extrusion of Ultra High Molecular Weight Polyethylene

Kostiantyn Vasylevskyi
University of New Hampshire
Department of Mechanical Engineering
33 Academic Way, Durham, NH 03824
kv1012@wildcats.unh.edu

Igor Tsukrov[1]
University of New Hampshire
Department of Mechanical Engineering
33 Academic Way, Durham, NH 03824
Igor.Tsukrov@unh.edu

Kateryna Miroshnichenko
University of New Hampshire
Department of Mechanical Engineering
33 Academic Way, Durham, NH 03824
km1180@wildcats.unh.edu

Stanislav Buklovskyi
University of New Hampshire
Department of Mechanical Engineering
33 Academic Way, Durham, NH 03824
sb1454@wildcats.unh.edu

Hannah Grover
Thayer School of Engineering at Dartmouth College
14 Engineering Drive Hanover, NH 03755
hannah.m.grover.th@dartmouth.edu

Douglas Van Citters
Thayer School of Engineering at Dartmouth College
14 Engineering Drive Hanover, NH 03755
Douglas.W.Van.Citters@dartmouth.edu

[1] Corresponding author

Journal of Manufacturing Science and Engineering. Received February 11, 2021;
Accepted manuscript posted May 10, 2021. doi:10.1115/1.4051189

ABSTRACT

Ultra-high molecular weight polyethylene (UHMWPE) used in biomedical applications, e.g. as a bearing surface in total joint arthroplasty, has to possess superior tribological properties, high mechanical strength, and toughness. Recently, equal channel angular extrusion (ECAE) was proposed as a processing method to introduce large shear strains to achieve higher molecular entanglement and superior mechanical properties of this material. Finite element analysis (FEA) can be utilized to evaluate the influence of important manufacturing parameters such as the extrusion rate, temperature, geometry of the die, back pressure, and friction effects. In this paper we present efficient FEA models of ECAE for UHMWPE.

Our studies demonstrate that the choice of the constitutive model is extremely important for the accuracy of numerical modeling predictions. Three considered material models (J2-plasticity, Bergstrom-Boyce, and the Three Network Model) predict different extrusion loads, deformed shapes and accumulated shear strain distributions. The work has also shown that the friction coefficient significantly influences the punch force and that the 2D plane strain assumption can become inaccurate in the presence of friction between the billet and the extrusion channel. Additionally, a sharp corner in the die can lead to the formation of the so-called "dead zone" due to a portion of the material lodging into the corner and separating from the billet. Our study shows that the presence of this material in the corner substantially affects the extrusion force and the resulting distribution of accumulated shear strain within the billet.

1. INTRODUCTION

Equal channel angular extrusion (ECAE) was initially proposed as a method to deliver large amounts of uniform shear deformation to a metal specimen in order to influence the material microstructure and improve its mechanical and physical properties, see for example [1]. This technique is widely used for metal alloys processing and is being actively developed and improved, see [2] , [3] and review [4].

Journal of Manufacturing Science and Engineering. Received February 11, 2021;
Accepted manuscript posted May 10, 2021. doi:10.1115/1.4051189

Originally developed for metals, ECAE is also being considered for processing of polymer materials to form oriented structures and improve properties, see [5]. One of the earliest numerical modeling studies on extrusion of polymer material (polycarbonate) was published in [6]. The authors assumed 2D plane strain and used a J2-Plasticity material model. More advanced 2D plane strain numerical simulations of the angular extrusion were performed in [7] and [8] for high density polyethylene (HDPE) material. These publications implemented a hypoelastic visco-plastic constitutive model to account for the strain rate sensitivity of the polymer. The authors investigated how the die geometry and number of passes affect stress and strain fields within the polymer billet. The experimental study on how angular extrusion affects mechanical properties of polypropylene (PP), supported by numerical modeling of the extrusion process, was reported in [9]. Similarly, numerical and experimental studies on the applicability of ECAE process and its influence on the properties and behavior of polypropylene and HDPE were presented in [10]. The authors performed a set of parametric numerical studies on the extrusion rate, billet-die friction coefficient, and back pressure sensitivity for PP and HDPE showing that those parameters are crucial.

Recently, ECAE was proposed as a means of achieving higher molecular entanglement and/or superior mechanical properties of ultra high molecular weight polyethylene (UHMWPE) [11] and UHMWPE-based composites [12]. The numerical modeling of the process could be used to better understand its mechanics and how it influences physical and mechanical properties of the resulting material. In particular, it can be used to evaluate the importance of the processing parameters such as friction between the billet and the die, extrusion rate, extrusion angle, back-pressure, and processing temperature. However, to the best of the authors' knowledge, there are no published results on the numerical simulations of the ECAE for UHMWPE material. This paper is based on the research presented at the IMECE 2020 conference [13]. It extends beyond the results published in the conference proceeding by including temperature-dependent simulations and providing comparison with available experimental data.

The paper is organized as follows, Section 2 describes the experimental set-up for the ECAE of UHMWPE and its implementation in finite element analysis (FEA). Three constitutive material models utilized in the extrusion simulations are presented in Section 3. Section 4 provides comparison of our modeling approach to the published results for the extrusion of high density polyethylene (HDPE). Section 5 presents several numerical studies including a comparison between 2D plane strain and 3D models, a friction sensitivity study, and a comparative analysis of the constitutive material models used for large deformations of polymers during extrusion. The issues related to the extrusion channel shape and the process temperature are also addressed in the section. Conclusions are provided in section 6.

2. FINITE ELEMENT MODEL OF EQUAL CHANNEL ANGULAR EXTRUSION EXPERIMENT

Finite element model has been developed for the ECAE process illustrated in Fig. 1. In this particular setup, a steel angular channel with a square cross-section of 50mm × 50mm and a sharp right-angle connection (Φ=90o, Ψ=0) is used. A set of heating cartridges is embedded into the channel walls to maintain constant temperature during the extrusion. An aluminum pressure punch which extrudes the material billet is velocity controlled and a back-pressure plate which delivers resistance to the billet motion in the horizontal part of the channel is force

Journal of Manufacturing Science and Engineering. Received February 11, 2021;
Accepted manuscript posted May 10, 2021. doi:10.1115/1.4051189

controlled in order to be able to prescribe desired extrusion rate and back-pressure. The virgin polymer powder is placed to the vertical portion of the channel and then compressed at elevated temperature of 162.5^{o}C for 2.5 hours for the purpose of polymer consolidation. A colored pigment can be added to layers of the powder to make the polymer billet striped and allow tracking its deformations. After that the specimen is extruded at elevated temperature 162.5oC and with the pressure punch velocity of 15 mm/min. Once the extrusion is complete, the billet is extracted from the horizontal part of the channel using a displacement-controlled extraction punch. More detailed description of the experimental set-up is given in [11] and [12].

The schematics provided in Fig. 1 illustrates the case when angle Ψ=0 (sharp corner). For extrusion of UHMWPE, this design of the die can lead to formation of the so-called "dead zone" – a portion of the material billet which gets stuck in the lower corner of the channel and eventually separates during the extrusion, see Fig. 2. To deal with this problem, the channel geometry can be improved by either increasing angle Φ (Φ>90^o), or introducing a smooth fillet in the lower corner by increasing angle Ψ (Ψ>0), or adding a mitre-fillet-like insert to the lower left corner of the die which can potentially prevent material from jamming and separating during the extrusion.

In the numerical models, the extrusion channel, pressure punch, back-pressure plate and the extraction punch are modeled as rigid surface contact bodies. The extrusion channel is fixed, the pressure punch has its vertical displacement and velocity prescribed, the back-pressure plate is force controlled and the extraction punch is displacement controlled. The extrusion billet is modeled using ~15 thousand 2D plane strain Herrmann quadrilateral finite elements in the case of 2D plane strain assumption and ~120 thousand 3D tetrahedral linear

Journal of Manufacturing Science and Engineering. Received February 11, 2021;
Accepted manuscript posted May 10, 2021. doi:10.1115/1.4051189

finite elements in the case of 3D simulations (Fig. 3). The mesh size for each model was chosen based on the tradeoff between successful convergence of the simulations and their computational efficiency.

The contact interaction between deformable finite elements and rigid contact bodies is modeled as bilinear shear friction sliding (see [14]). Extrusion and extraction processes are simulated by two consecutive load cases. The extrusion takes 600s which corresponds to the experimental extrusion time. All simulations are performed using MSC Marc Mentat software (https://www.mscsoftware.com/product/marc).

3. MATERIAL MODELS FOR EXTRUSION OF ULTRA HIGH MOLECULAR WEIGHT POLYETHYLENE

One of the important steps in numerical modeling of such a complex process as ECAE of a polymeric material is to pick an adequate constitutive material model. We begin with the assumptions that the billet material will be non-porous before the beginning of the extrusion process due to compaction at elevated temperature, and its behavior can be described by continuum solid mechanics equations. The material extrusion is performed at elevated temperatures, so the thermal sensitivity of a chosen material model is especially important. There are two approaches to include temperature dependence of the material behavior. The first approach is to perform characterization tests for the material at each level of temperature which the material is processed at. Such an approach is needed when the material model does not directly account for thermal sensitivity, for example, J_2-Plasticity or Bergstrom-Boyce (BB) [15]. The second approach is to perform characterization experiments at certain levels of

Journal of Manufacturing Science and Engineering. Received February 11, 2021;
Accepted manuscript posted May 10, 2021. doi:10.1115/1.4051189

temperature, and use them to calibrate the material's temperature-dependent response. This approach is used when the constitutive model explicitly accounts for thermal sensitivity of the material properties. Additionally, the material model has to be applicable to large compressive and shear deformations of the polymer. It has to allow for accounting of the strain rate sensitivity of the material. It also needs to be easily calibrated based on limited experimental data (usually simple tension and compression tests).

The J_2-Plasticity (J_2) model is often the simplest choice as in [6] and [16] where it is used for modeling of ECAE of polycarbonate and HDPE. According to the model, the yielding in the material occurs when the second invariant of deviatoric stress (J_2) reaches a critical value. Expressing J_2 in terms of principal stresses σ_1, σ_2 and σ_3, the yield criterion can be written as follows: $\bar{\sigma} = \sigma_y$, where σ_y is the tensile yield strength and $\bar{\sigma} = \frac{1}{\sqrt{2}}\sqrt{(\sigma_1 - \sigma_2)^2 + (\sigma_2 - \sigma_3)^2 + (\sigma_3 - \sigma_1)^2}$ is the effective von Mises stress. In the numerical implementations of the model, the evolution of the yield stress is usually specified as a piecewise linear function of the equivalent plastic strain $\bar{\varepsilon}_p$ (https://www.mscsoftware.com/product/marc). However, the J_2 material model was developed for metallic materials and hence is usually not suitable for highly rate and temperature dependent polymers [17]. In addition, plastic behavior of polymeric materials is dependent on the first invariant of stress tensor (see for example [18], [19] and [20]) which is not reflected by J_2 - model.

A more advanced option is the Bergstrom-Boyce (BB) model [15]. This model was developed for elastomers, however, it can be applied to UHMWPE as its high molecular weight causes the

Journal of Manufacturing Science and Engineering. Received February 11, 2021;
Accepted manuscript posted May 10, 2021. doi:10.1115/1.4051189

polymer chains to entangle and hence act like crosslinks producing a pseudo-elastomeric response of the amorphous region. The model includes strain rate sensitivity of the polymer and can be calibrated with only two loading-unloading tests performed at different strain rates. Obviously, having more experimental data will improve its accuracy. This model is usually included in commercial FE software packages which makes it easy to implement. In addition, the Bergstrom-Boyce model was validated for UHMWPE [17] in several simple mechanical tests (tension and compression). According to BB, the mechanical response of a material is governed by two networks A and B acting in parallel (see Fig. 4). The first network A controls the equilibrium behavior of the material and the second network B governs the time-dependent deviation from equilibrium. The total Cauchy stress is a sum of stresses acting on networks A and B. Appendix A provides explicit expressions for the stresses acting on networks A and B along with the governing equations for the viscous response of network B. The major disadvantage of the model is its inability to directly take the temperature sensitivity into account requiring additional sets of experiments at each temperature of interest.

The Three Network Model (TNM) presented in [21] explicitly includes dependence on both strain rate and temperature sensitivity. It has been developed specifically for UHMWPE and has shown good agreement with the experimental data. The initial viscoplastic response of the material is governed by two energy activation mechanisms which correspond to amorphous and semicrystalline domains and the large strain behavior is governed by entropic resistance. Rheologically, the model consists of three networks A, B and C which act in parallel (Fig. 5). The network A is a temperature dependent version of an eight-chain model similar to [22] and [23]. The B network is similar to network A except that the effective bulk modulus of the network

Journal of Manufacturing Science and Engineering. Received February 11, 2021;
Accepted manuscript posted May 10, 2021. doi:10.1115/1.4051189

evolves with plastic strain which allows the transition from initial yielding to large strains flow to be captured. The network C is governed by an eight-chain model including dependence on stretch tensor invariants similarly to the Mooney-Rivlin model with non-Gaussian chain statistics [24], [25]. The total stress acting on the model is a sum of the stresses acting on each network A, B and C. Appendix B provides explicit expressions for the stresses acting on networks A, B and C along with the governing equations for the viscous response of networks A and B. The challenge for this model is that it requires a significant number of characterization tests to calibrate and implement due to a large number of material parameters.

Three constitutive models (J_2, BB, and TNM) were implemented in the MSC Marc simulations utilizing add-on software PolyUMod (https://polymerfem.com/polyumod/). To calibrate material models, we used MCalibration software (https://polymerfem.com/mcalibration/) based on a set of characterization uniaxial experiments published for HDPE in [7] and for UHMWPE GUR 1050 in [26].

4. VALIDATION FOR EXTRUSION OF HIGH DENSITY POLYETHYLENE

As part of the validation effort, we compared predictions by our models with the published data for ECAE of HDPE, see [7]. We constructed a 2D plane strain finite element model based on the description provided in [7]. A billet of 10mm × 10mm × 100mm is extruded through a rigid right-angle channel with $\Phi=90^o$ and $\Psi=0$ and zero friction at the contact surface between the billet and the die. The extrusion is performed at constant rate of 6 mm/min and at two values of temperature (25^{o}C and 60^{o}C). In our comparative simulations, we utilized the J_2-Plasticity model and calibrated it using the material characterization data published in the same paper ([7]). The

Journal of Manufacturing Science and Engineering. Received February 11, 2021;
Accepted manuscript posted May 10, 2021. doi:10.1115/1.4051189

obtained model parameters are summarized in Table I where E is the Young's modulus, v is the Poisson's ratio, ε_p is the equivalent plastic strain, and $\bar{\sigma}_Y$ is the equivalent material yield stress.

Fig. 6 shows a comparison of the predictions for the time history of the extrusion punch force in the experiment conducted at 25°C and 60°C.

The relative percentage difference as compared to the peak load of the "published model" and the steady extrusion force were calculated to evaluate the level of agreement. The difference between the "present model" and the "published model" peak loads is 26% and 3.2% whereas the difference at the steady portion of the curves (at 400s) is 6% and 4.7% for 25°C and 60°C, respectively. Thus, it can be seen that predictions practically coincide for 60°C. For the 25°C extrusion, a noticeable difference is observed in the peak load. Note that in [7], the authors used a different material model (hypoelastic viscoplastic) which directly accounts for rate sensitivity requiring sets of characterization experiments at all considered temperatures. Apparently, utilizing J_2 instead of their model leads to a later transition from compression to the shearing phase in the simulated extrusion process at 25°C.

5. RESULTS AND DISCUSSION

We performed a set of parametric studies for numerical models simulating ECAE process of the UHMWPE GUR 1050 material. This material has a crystallinity level of 50.4%$\pm$3.3%, density 0.933 g/cm^3 and 5.5-6$\times 10^6$g/mole molar mass as described in [26]. Section 5.1 presents results on the sensitivity of the predictions to the billet-die friction parameters, namely, the friction coefficient between the billet and the die. In section 5.2 we investigate the accuracy of the 2D plane strain assumption by comparing two-dimensional and three-dimensional modeling

Journal of Manufacturing Science and Engineering. Received February 11, 2021;
Accepted manuscript posted May 10, 2021. doi:10.1115/1.4051189

results. Section 5.3 provides an insight on the importance of the proper choice of the material constitutive model. Section 5.4 considers how the introduction of a triangular prismatic insert to the lower corner of the channel changes the force applied to the pressure punch by partially replicating the formation and separation of the dead zone and its subsequent impact on channel geometry.

The simulations were performed for the extrusion punch velocity of 15 mm/min which corresponds to the shear strain rate on the order of 0.05 s^{-1}, and a back pressure of 36 MPa. Five different values of the friction coefficient and four different values of the extrusion temperature were considered.

5.1 Friction Study

Friction between the die and the billet plays a significant role in the extrusion process, see [27]. A parametric study was conducted in order to investigate how the friction coefficient μ influences the predictions for the extrusion forces during ECAE. A set of 3D FE simulations using the 3D J_2-Plasticity model was performed with various values of friction coefficient: μ = 0.01, 0.05, 0.1, 0.15 and 0.2. Note that in the simulations, μ = 0.01 corresponds to the frictionless sliding of the billet within the channel. The small number is chosen instead of μ = 0 to improve numerical convergence. The use of frictionless contact is justified by the experimental data published in [28] where the authors show that friction can be neglected if mean contact pressure is larger than 30 MPa. The value μ = 0.2 was chosen as a maximum value based on the data reported in [29].

Journal of Manufacturing Science and Engineering. Received February 11, 2021;
Accepted manuscript posted May 10, 2021. doi:10.1115/1.4051189

Fig. 7 confirms that the friction coefficient is an important parameter and must be accurately evaluated for realistic simulation of the extrusion process. As can be seen by comparing with no friction results (μ=0.01), the amount of force needed to overcome friction during the extrusion phase of the process reaches 30% of the total force for μ=0.1 and 80% for μ=0.2.

5.2 2D vs. 3D

3D FE models contain a significant number of finite elements which can result in long simulation times and accumulation of a round-off error when modeling such highly nonlinear process as ECAE for UHMWPE. A 2D plane strain approximation can be a good option to reduce computational effort when the distribution of stresses and strains does not significantly vary in the direction normal to the lateral sides of the extrusion channel. Thus, a numerical study was performed to evaluate applicability of 2D plane strain assumption for ECAE of UHMWPE. In the presented simulations, the J_2-Plasticity model was used because it is the simplest to implement. Since the plane strain assumption is geometrical and does not involve any constraints on physical behavior of the material, the obtained results will also be applicable to more complex material models.

As seen in Fig. 8, the predicted deformed shapes of the extracted billets are similar for 2D and 3D simulations. However, as shown in Fig. 9, the punch force vs. displacement curves for 3D and 2D are not similar when the friction coefficient μ is not negligible. The 3D model predicts a larger punch force which can be explained by the contribution of friction between the billet and the side walls of the extrusion channel. If the friction is small (μ=0.01), the difference

Journal of Manufacturing Science and Engineering. Received February 11, 2021;
Accepted manuscript posted May 10, 2021. doi:10.1115/1.4051189

between 2D and 3D predictions decreases significantly. This means that in the case of significant friction, the 2D assumption might become inaccurate and 3D modeling has to be considered.

5.3 Sensitivity to the Choice of the Material Model

A set of 2D plane strain finite element simulations was conducted to evaluate performance of three different constitutive models, J_2, BB, and TNM. All three material models were calibrated using experimental data from [26] assuming that the process is performed at room temperature (20°C). Note that this temperature regime is not typical for processing of polymer materials and was used only to investigate general trends in the models' predicting abilities as applied to UHMWE. The simulations were performed with friction coefficient μ=0.01 representing frictionless sliding of the billet within the channel.

Fig. 10 compares the deformed shapes predicted by all considered material models with the actual shape of the UHMWPE billet extracted from the angular channel after the extrusion. Based on the mutual orientation of the blue stripes within the billet and the outline of the deformed shape, the predictions by BB and TNM models appear to be closer to the experiment than the J_2-Plasticity model. However, there is still a noticeable discrepancy between the actual billet and the predictions by BB and TNM exhibited by lower curvature and higher inclination angle of blue stripes in the numerical results. We attribute this discrepancy to formation of the "dead zone" during the actual extrusion process that was not included in the numerical models. Another potential reason is that the constitutive models were not calibrated for the process temperature of 162.5°C.

Journal of Manufacturing Science and Engineering. Received February 11, 2021;
Accepted manuscript posted May 10, 2021. doi:10.1115/1.4051189

The punch force vs. displacement plot shown in Fig. 11 supports the observations made based on the deformed shapes comparison. Namely, the J_2-Plasticity model performs differently from BB and TNM. It predicts that a significantly larger load is needed to perform the extrusion which can be explained by linear hardening of the material in the model but is not the case for the considered polymer. At the same time, BB and TNM models have similar predictions for both the deformed shape and the punch force.

Fig. 12 shows the distribution of the maximum absolute value of shear strain experienced by the material during the ECAE process as predicted by the J_2, BB, and TNM material models. This parameter is important because it could be correlated with changes in molecular entanglement densities and/or material properties of UHMWPE. It can be seen that, similarly to the force-displacement curves, the BB and TNM models predict comparable levels of shear strain, while the strains predicted by J_2 are lower and more uniform.

5.4 Dead Zone Study. Process Temperature Influence

The results presented in 5.1-5.3 assume that the material stays continuous even at high levels of stresses with no separation or damage. Because of this, the punch force-displacement curves (Fig. 6 and Fig. 11) exhibit a well pronounced hill when the material is pulled from the sharp lower corner of the die. However, our experiments show that formation of the “dead zone” in the corner results in separation of the portion of the billet. It is presently challenging to model separation of material (propagation of crack or damage) directly as the proper fracture (or damage) initiation parameters for UHMWPE subjected to high compressive and shear stresses at elevated temperature are not available.

Journal of Manufacturing Science and Engineering. Received February 11, 2021;
Accepted manuscript posted May 10, 2021. doi:10.1115/1.4051189

To evaluate the extrusion in the absence of material fracture, we considered modification of the extrusion channel model by a mitre-fillet-like insert preventing formation of a dead zone by mimicking its shape. The modified extrusion channel and the insert are shown in Fig. 13. The dimensions of the insert are based on the size of the separated material portion. Note that introduction of the insert in our models was not aimed to provide justification for change of the actual die shape but rather to observe the effect of the dead zone formation on the punch force and the accumulated maximum shear strain in the material. A comprehensive numerical study on how the geometric shape of the extrusion channel influences the billet damage level during ECAE is shown for example in [30].

A set of numerical simulations was performed with the models incorporating the triangular insert to investigate its influence on the deformed shape of the billet, extrusion force, and maximum shear strains. Fig. 14 (A) shows comparison of the deformed shape of the billet after the extrusion with and without the insert. It can be seen that the introduction of the insert results in the outline of the billet becoming more similar to what is observed in the experiment, see the lower surface of the billet. Also, the orientation of the stripes corresponds better to the experimental image. However, there is still a noticeable difference between the experimental and predicted billets, especially at the upper surface of the deformed shape. The curvature of the blue stripes at the top surface of actual billet is likely due to severe local plastic deformations caused by the sharp upper corner of the die not captured by the FE models. The prediction of the extrusion load gets affected as well, see Fig. 14 (B). The bump in the force around 40 mm of the punch displacement, corresponding to the material getting stuck at the

Journal of Manufacturing Science and Engineering. Received February 11, 2021;
Accepted manuscript posted May 10, 2021. doi:10.1115/1.4051189

lower corner of the billet, disappears and the load drops at the stable portion of the curve by 30kN.

Fig. 15 shows the prediction of the maximum accumulated shear strain in the UHMWPE billet with and without triangular insert. According to the prediction, the introduction of the triangular insert significantly lowers the maximum shear stain throughout the billet (roughly two times) and results in a more uniform strain distribution. Accurately predicting, maximizing, and ensuring homogeneity of this effect is crucial as shear deformation under these conditions is hypothesized to fundamentally alter the microstructure and therefore the mechanical properties.

Another important parameter for ECAE of UHMWPE is the processing temperature. As stated above, all of the material models were calibrated for UHMWPE GUR 1050 using the experimental data from [26]. The J_2 and BB models do not include the temperature dependence of material properties (even though it can be incorporated by conducting characterization experiments for temperatures of interest). Unlike the J_2 and BB models, TNM allows explicit incorporation of temperature dependence. However, the experiments reported in [26] were performed at two values of temperature only (20^{o}C and 37^{o}C). In contrast, the actual extrusion process was conducted at a temperature of 162.5^{o}C for which the material characterization data is not presently available. Since the material model was calibrated for much lower temperatures, the numerical process loses its stability for temperatures above 140^{o}C. Thus, to investigate the thermal sensitivity of the extrusion process, we limited the range of considered temperatures to 20^{o}C – 140^{o}C. We are aiming not to exactly match experimental data but rather

Journal of Manufacturing Science and Engineering. Received February 11, 2021;
Accepted manuscript posted May 10, 2021. doi:10.1115/1.4051189

observe the trends in the predicted response. For this purpose, we report force-displacement curves for the extrusion process as simulated using TNM at 20°C, 90°C, and 140°C.

Fig. 16 compares the predictions for punch force as a function of the punch displacement to the actual experimental data. As seen in this image, the extrusion force drops by almost a third of what is predicted by the model at 20°C when the temperature is increased to 140°C. Since the constitutive model was calibrated using data for much lower temperatures, the predicted force at 140°C is lower than measured even though the experimental measurements were taken at 162.5°C. This proves that the proper reflection of the thermal sensitivity of the material properties is crucial for accurate modeling of ECAE process at elevated temperatures.

6. CONCLUSIONS

An efficient numerical procedure was developed to simulate ECAE of UHMWPE material in order to better understand the mechanics of the process and improve the processing parameters with the goal of achieving superior mechanical properties of UHMWPE. Three constitutive material models (J_2, BB and TNM), calibrated using published characterization experiments for GUR 1050 UHMWPE [26], were utilized in the simulations. A set of parametric studies was performed to investigate how numerical predictions are affected by friction parameters, geometrical assumptions (2D vs. 3D), constitutive model choice, "dead zone" formation, and process temperature.

We demonstrated that the value of the friction coefficient significantly affects the predicted extrusion punch force. For example, if the friction coefficient is increased from μ=0.01 to μ=0.2, the force applied to the extrusion punch increases by 80%.

Journal of Manufacturing Science and Engineering. Received February 11, 2021;
Accepted manuscript posted May 10, 2021. doi:10.1115/1.4051189

The geometrical assumption study has shown that the 2D plane strain assumption can be a good option for the ECAE process simulation if the friction between the billet and the die is small or can be completely neglected. However, if the friction is not small then the 2D assumption becomes inaccurate.

The applicability of three constitutive models (J_2, BB and TNM) to the prediction of the UHMWPE behavior during ECAE process was investigated. It has been shown that the prediction based on J_2-Plasticity is not in good agreement with the experimental results, both by deformed shape and punch force comparison. In addition, the J_2 model does not account for the material strain rate and temperature sensitivity and hence cannot accurately predict the polymer behavior. In contrast, two other material models, the BB and TNM, showed similar performance and their utilization resulted in a more accurate prediction of the billet shapes after extrusion and of the punch forces. Even though both models account for the strain rate sensitivity of the UHMWPE, only TNM explicitly includes temperature in its constitutive equations. So, it comes to a trade-off between running a set of characterization tests at each value of temperature to calibrate the BB model and calibrating the more advanced TNM which requires more extensive characterization testing and includes more material parameters. Another factor to consider is that BB model is included in most commercial FE software packages.

Note that our simulations are performed at the macroscale; they do not explicitly include microstructure of the material (crystallinity, molecular entanglement, possible porosity, etc.) and its evolution. Incorporation of microstructure evolution (which is usually implemented by assigning the material properties at each integration point of the FE mesh based on changes in the associated representative volume element during each time increment) would improve

Journal of Manufacturing Science and Engineering. Received February 11, 2021;
Accepted manuscript posted May 10, 2021. doi:10.1115/1.4051189

both accuracy and spatial resolution of the models. At the same time, such multiscale simulations would require more information on macromolecular dynamics and significant computational resources.

During extrusion, it is possible that a portion of material gets stuck in the sharp corner ("dead zone") of the die leading to an increased punch force and possible material separation. Modeling of the material separation is challenging as it is unclear which damage initiation and/or fracture propagation criteria would be appropriate. We proposed to avoid modeling the separation of the "dead zone" by introducing a mitre-fillet-like insert in the lower corner of the extrusion channel. This resulted in the improved prediction of the deformed shape of the billet. The prediction of the punch force as compared to the experimental data improved both qualitatively and quantitatively (by 24%). However, this measure is artificial and can be used only if the simulation of the actual "dead zone" formation and material separation is not feasible.

The influence of the processing temperature on the numerical predictions for the ECAE of UHMWPE was investigated. As the TNM constitutive model was calibrated using characterization experimental data obtained at much lower temperatures than the actual level during the extrusion, the prediction was not aimed to obtain an exact match with the experimental data but observe the trend. It has been shown that with the increase in temperature the extrusion force drops significantly.

One of the important simulation results is the distribution of maximum accumulated shear strains in extruded UHMWPE billet. It can be used to better understand how the polymer chain entanglement level may vary within the billet and how the processing parameters (such as

Journal of Manufacturing Science and Engineering. Received February 11, 2021;
Accepted manuscript posted May 10, 2021. doi:10.1115/1.4051189

temperature, extrusion rate, back pressure, friction, etc.) affect the local microstructure. It has been shown that the most influential factor is the presence of the "dead zone" as it significantly affects the magnitude and distribution of the maximum shear strain. Namely, when the triangular insert is introduced, the predicted magnitude of the shear strain is roughly two times lower as compared to the model without the insert, but its distribution is much more uniform. The information on distribution of accumulated shear strain could be a powerful means for predicting localized alterations to polymer chain conformation as well as mechanical properties within experimentally produced billets.

ACKNOWLEDGMENTS

The authors would like to thank Dr. Jorgen Bergström for his help with accessing the constitutive material modeling software.

FUNDING

This research is supported by a National Science Foundation EPSCoR award (#1757371).

Journal of Manufacturing Science and Engineering. Received February 11, 2021;
Accepted manuscript posted May 10, 2021. doi:10.1115/1.4051189

Appendix A. Bergstrom-Boyce Material Model

This model has been originally proposed in [15] and widely used for modeling of polymeric materials' behavior, see for example [17], [31]. It can directly account for strain rate sensitivity of the material. However, for temperature dependent response, this model requires characterization experiments at each value of temperature of interest.

In this model, total Cauchy stress $\boldsymbol{\sigma}$ is a sum of the Cauchy stresses acting on networks A and B:

$$\boldsymbol{\sigma} = \boldsymbol{\sigma}_A + \boldsymbol{\sigma}_B. \tag{1}$$

The Cauchy stress acting on network A is as

$$\boldsymbol{\sigma}_A = \frac{\mu_A}{J\overline{\lambda^*}} \frac{L^{-1}\left(\overline{\lambda^*}/\lambda_A^{lock}\right)}{L^{-1}\left(1/\lambda_A^{lock}\right)} \mathrm{dev}(\mathbf{B}_{\boldsymbol{A}}^*) + \kappa(\ln J)\mathbf{I} \tag{2}$$

where μ_A is the initial shear modulus, λ_A^{lock} is the limiting chain stretch, κ is the bulk modulus, $\mathbf{B}_{\boldsymbol{A}}^* = (J)^{-2/3}\mathbf{F}_{\boldsymbol{A}}\mathbf{F}_A^T$ is the distortional portion of the left Cauchy-Green tensor, $\mathbf{F}_{\boldsymbol{A}}$ is deformation gradient, $\overline{\lambda^*} = \sqrt{tr(\mathbf{B}_{\boldsymbol{A}}^*)/3}$ is the effective chain stretch, $J = \det(\mathbf{F}_{\boldsymbol{A}})$ is the volume change, L^{-1} is the inverse Langevin function.

The Cauchy stress on network B is expressed as

$$\boldsymbol{\sigma}_B = \frac{\mu_B}{J_B^e\overline{\lambda_B^{e*}}} \frac{L^{-1}\left(\overline{\lambda_B^{e*}}/\lambda_B^{lock}\right)}{L^{-1}\left(1/\lambda_B^{lock}\right)} \mathrm{dev}(\mathbf{B}_{\boldsymbol{B}}^{\boldsymbol{e}*}) + \kappa(\ln J_B^e)\mathbf{I} \tag{3}$$

where $J_B^e = \det(\boldsymbol{F}_B^e)$ is the elastic volume change of the network B, $\overline{\lambda_B^{e*}} = \sqrt{tr(\mathbf{B}_{\boldsymbol{B}}^{\boldsymbol{e}*})/3}$ is chain stretch in the elastic part of network B, $\lambda_B^{lock} = \lambda_A^{lock}$is the limiting chain stretch $\mathbf{B}_B^{e*} = (J_B^e)^{-2/3}\mathbf{F}_B^e\mathbf{F}_B^{e^T}$ is the finger (left Cauchy-Green) tensor of the elastic part of network B, $\mathbf{F}_B^e$ is the elastic part of the deformation gradient tensor.

The viscous part of the network "B" is governed by the effective strain rate:

$$\dot{\gamma}_B = \left(\overline{\lambda_B^p} - 1\right)^C \left(\frac{\tau}{\tau_{base}}\right)^m \tag{4}$$

where $\overline{\lambda_B^p} = \sqrt{\mathrm{tr}(\mathbf{B}_B^p)/3}$ is the viscoplastic chain stretch, $\tau = \left(\mathrm{tr}(\boldsymbol{\sigma}'_B \boldsymbol{\sigma}'_B)\right)^{1/2}$ is the effective stress driving the viscous flow, and the deviatoric part of the Cauchy stress acting on the network B $\boldsymbol{\sigma}'_B$ is expressed as $\boldsymbol{\sigma}'_B = \mu_B \mathrm{dev}(\mathbf{B}_B^e)$. In Eq. (4), μ_B is the shear modulus of the network B and C, m, τ_{base} are the material parameters.

Appendix B. Three-Network Material Model

This model has been originally proposed in [21] and widely used for modeling of polymeric materials' behavior including temperature sensitivity of the material response, see, for example, [32] and [33]. It directly takes into account both strain rate and temperature dependence.

In this model the total Cauchy stress $\boldsymbol{\sigma}$ is a sum of the Cauchy stresses acting on networks A, B and C:

$$\boldsymbol{\sigma} = \boldsymbol{\sigma}_A + \boldsymbol{\sigma}_B + \boldsymbol{\sigma}_C. \tag{5}$$

The Cauchy stress acting on the network A is given by

$$\boldsymbol{\sigma}_A = \frac{\mu_A}{J_A^e \overline{\lambda_A^{e*}}}\left(1 + \frac{\theta - \theta_0}{\hat{\theta}}\right) \frac{L^{-1}\left(\overline{\lambda_A^{e*}}/\lambda_A^{lock}\right)}{L^{-1}\left(1/\lambda_A^{lock}\right)} \mathrm{dev}(\mathbf{B}_A^{e*}) + \kappa(J_A^e - 1)\mathbf{I} \tag{6}$$

where $J_A^e = \det(\boldsymbol{F}_A^e)$ is the elastic volume change in the network A, μ_A is the initial shear modulus, λ_A^{lock} is the limiting chain stretch, θ is the current temperature, θ_0 is the reference temperature, $\hat{\theta}$ is the is a material parameter specifying the temperature response of the stiffness, $\mathbf{B}_A^e = (J_A^e)^{-2/3} \mathbf{F}_A^e \mathbf{F}_A^{e^T}$ is the finger (left Cauchy-Green) tensor of the elastic part of network A, $\overline{\lambda_A^{e*}} = \sqrt{tr(\mathbf{B}_A^{e*})/3}$ is the is the effective chain stretch based on the eight-chain topology assumption, κ is the bulk modulus, L^{-1} is the inverse Langevin function, $\mathbf{I}$ is the unit tensor.

The viscous part of the network A is governed by the effective strain rate:

$$\dot{\gamma}_A = \dot{\gamma}_0 \left(\frac{\tau_A}{\hat{\tau}_A + \alpha R(p_A)}\right)^{m_A} \cdot \left(\frac{\theta}{\theta_0}\right)^n \tag{7}$$

where $\dot{\gamma}_0 = 1/s$ is the dimensional consistency constant, $\tau_A = \left(\mathrm{tr}(\boldsymbol{\sigma}'_A \boldsymbol{\sigma}'_A)\right)^{1/2}$ is the effective stress, $p_A = -\frac{(\boldsymbol{\sigma}_A)_{11} + (\boldsymbol{\sigma}_A)_{22} + (\boldsymbol{\sigma}_A)_{33}}{3}$ is the hydrostatic pressure, $R(x) = (x + |x|)/2$ is the ramp function, $\hat{\tau}_A$, α, m_A, n are the material parameters.

The Cauchy stress acting on network B is governed by the following equation:

$$\boldsymbol{\sigma}_B = \frac{\mu_B}{J_B^e \overline{\lambda_B^{e*}}} \left(1 + \frac{\theta - \theta_0}{\hat{\theta}}\right) \frac{L^{-1}\left(\overline{\lambda_B^{e*}}/\lambda_B^{lock}\right)}{L^{-1}\left(1/\lambda_B^{lock}\right)} \mathrm{dev}(\mathbf{B}_B^{e*}) + \kappa(J_B^e - 1)\mathbf{I} \tag{8}$$

where $J_B^e = \det(\boldsymbol{F}_B^e)$ is the elastic volume change in the network B, $\mathbf{B}_B^e = (J_B^e)^{-2/3}\mathbf{F}_B^e \mathbf{F}_B^{eT}$ is the finger (left Cauchy-Green) tensor of the elastic part of network B, $\overline{\lambda_B^{e*}} = \sqrt{tr(\mathbf{B}_B^{e*})/3}$ is the effective chain stretch based on the eight-chain topology assumption.

Effective shear modulus μ_B evolves from μ_{Bi} to μ_{Bf} with plastic strain according to the following rule:

$$\dot{\mu_B} = -\beta(\mu_B - \mu_{Bf})\dot{\gamma_A} \tag{9}$$

where $\dot{\gamma_A}$ is the viscoplastic flow rate.

Similarly to the network A, the viscous flow rate for network B is given by

$$\dot{\gamma}_B = \dot{\gamma}_0 \left(\frac{\tau_B}{\hat{\tau}_B + \alpha R(p_B)}\right)^{m_B} \cdot \left(\frac{\theta}{\theta_0}\right)^n \tag{10}$$

where $\tau_B = \left(\mathrm{tr}(\boldsymbol{\sigma}'_B \boldsymbol{\sigma}'_B)\right)^{1/2}$ is the effective stress, $p_A = -\frac{(\boldsymbol{\sigma}_B)_{11} + (\boldsymbol{\sigma}_B)_{22} + (\boldsymbol{\sigma}_B)_{33}}{3}$, $\hat{\tau}_B$, m_B, are the material parameters.

Journal of Manufacturing Science and Engineering. Received February 11, 2021;
Accepted manuscript posted May 10, 2021. doi:10.1115/1.4051189

The Cauchy stress in the third network C is

$$\boldsymbol{\sigma}_C = \frac{1}{1+q}\left[\frac{\mu_C}{J\overline{\lambda^*}}\left(1+\frac{\theta-\theta_0}{\hat{\theta}}\right)\frac{L^{-1}\left(\overline{\lambda^*}/\lambda_C^{lock}\right)}{L^{-1}\left(1/\lambda_C^{lock}\right)}\mathrm{dev}(\mathbf{B}^*) + \kappa(J-1)\mathbf{I} + q\,\frac{\mu_C}{J}\left(I_1^*\mathbf{B}^* - \frac{2I_2^*}{3}\mathbf{I} - (\boldsymbol{B}^*)^{\mathbf{2}}\right)\right], \quad (11)$$

where μ_C is the initial shear modulus, $\mathbf{B}^* = J^{-2/3}\mathbf{F}\mathbf{F}^{\mathrm{T}}$ is the Cauchy-Green deformation tensor, $\overline{\lambda}^* = \sqrt{tr(\mathbf{B}^*)/3}$ is the effective chain stretch, q is the material parameter, I_1^* and I_2^* are the stretch tensor first and second invariants.

REFERENCES

[1] Segal, V. M., 1995, “Materials Processing by Simple Shear,” Mater. Sci. Eng. A, **197**(2), pp. 157–164.

[2] Beyerlein, I. J., and Tóth, L. S., 2009, “Texture Evolution in Equal-Channel Angular Extrusion,” Prog. Mater. Sci., **54**(4), pp. 427–510.

[3] Djavanroodi, F., Omranpour, B., Ebrahimi, M., and Sedighi, M., 2012, “Designing of ECAP Parameters Based on Strain Distribution Uniformity,” Prog. Nat. Sci. Mater. Int., **22**(5), pp. 452–460.

[4] Segal, V., 2020, “Equal-Channel Angular Extrusion (ECAE): From a Laboratory Curiosity to an Industrial Technology,” Metals (Basel)., **10**(2).

[5] Beloshenko, V. A., Voznyak, Y. V., Reshidova, I. Y., Naït-Abdelaziz, M., and Zairi, F., 2013, “Equal-Channel Angular Extrusion of Polymers,” J. Polym. Res., **20**(12).

[6] Sue, H. J., Dilan, H., and Li, C. K. Y., 1999, “Simple Shear Plastic Deformation Behavior of Polycarbonate Plate Due to the Equal Channel Angular Extrusion Process. I: Finite Element Methods Modeling,” Polym. Eng. Sci., **39**(12), pp. 2505–2515.

[7] Aour, B., Zaïri, F., Naït-Abdelaziz, M., Gloaguen, J. M., Rahmani, O., and Lefebvre, J. M., 2008, “A Computational Study of Die Geometry and Processing Conditions Effects on Equal Channel Angular Extrusion of a Polymer,” Int. J. Mech. Sci., **50**(3), pp. 589–602.

[8] Aour, B., Zaïri, F., Naït-Abdelaziz, M., Gloaguen, J. M., and Lefebvre, J. M., 2009, “Finite Element Analysis of Plastic Strain Distribution in Multipass ECAE Process of High Density Polyethylene,” J. Manuf. Sci. Eng. Trans. ASME, **131**(3), pp. 0310161–03101611.

[9] Boulahia, R., Gloaguen, J. M., Zaïri, F., Naït-Abdelaziz, M., Seguela, R., Boukharouba, T., and Lefebvre, J. M., 2009, “Deformation Behaviour and Mechanical Properties of Polypropylene Processed by Equal Channel Angular Extrusion: Effects of Back-Pressure and Extrusion Velocity,” Polymer (Guildf)., **50**(23), pp. 5508–5517.

[10] Aour, B., Zaïri, F., Boulahia, R., Naït-Abdelaziz, M., Gloaguen, J. M., and Lefebvre, J. M., 2009, “Experimental and Numerical Study of ECAE Deformation of Polyolefins,” Comput. Mater. Sci., **45**(3), pp. 646–652.

[11] Reinitz, S. D., Engler, A. J., Carlson, E. M., and Van Citters, D. W., 2016, “Equal Channel Angular Extrusion of Ultra-High Molecular Weight Polyethylene,” Mater. Sci. Eng. C, **67**, pp. 623–628.

[12] Cook, D. J., Chun, H. H., and Van Citters, D. W., 2019, “Mechanical and Electrical Characterization of Two Carbon/Ultra High Molecular Weight Polyethylene Composites Created Via Equal Channel Angular Processing,” J. Eng. Mater. Technol. Trans. ASME, **141**(2), pp. 1–7.

[13] Vasylevskyi, K., Miroshnichenko, K., Buklovskyi, S., Tsukrov, I., Grover, H., and Citters, D. Van, 2020, “On Numerical Modeling of Equal Channel Angular Extrusion of Ultra High Molecular Weight Polyethylene,” Proc. ASME 2020 Int. Mech. Eng. Congr. Expo. IMECE2020.

[14] 2019, “Marc® 2019 Volume A: Theory and User Information,” p. 1039.

[15] Bergström, J. S., and Boyce, M. C., 1998, “Constitutive Modeling of the Large Strain Time-Dependent Behavior of Elastomers,” J. Mech. Phys. Solids, **46**(5), pp. 931–954.

[16] Wu, X., Pu, L., Xu, Y., Shi, J., Liu, X., Zhong, Z., and Luo, S. N., 2018, “Deformation of High Density Polyethylene by Dynamic Equal-Channel-Angular Pressing,” RSC Adv., **8**(40), pp. 22583–22591.

[17] Bergström, J. S., Kurtz, S. M., Rimnac, C. M., and Edidin, A. A., 2002, “Constitutive Modeling of Ultra-High Molecular Weight Polyethylene under Large-Deformation and Cyclic Loading Conditions,” Biomaterials, **23**(11), pp. 2329–2343.

[18] Ainbinder, S. B., Laka, M. G., and Maiors, I. Y., 1965, “Effect of Hydrostatic Pressure on Mechanical Properties of Plastics,” Polym. Mech., **1**(1), pp. 50–55.

[19] Laka, M. G., and Dzenis, A. A., 1967, “Effect of Hydrostatic Pressure on the Tensile Strength of Polymer Materials,” Polym. Mech., **3**(6), pp. 685–687.

[20] Mears, D. R., Pae, K. D., and Sauer, J. A., 1969, “Effects of Hydrostatic Pressure on the Mechanical Behavior of Polyethylene and Polypropylene,” J. Appl. Phys., **40**(11), pp. 4229–4237.

[21] Bergström, J. S., and Bischoff, J. E., 2010, “An Advanced Thermomechanical Constitutive Model for UHMWPE,” Int. J. Struct. Chang. Solids, **2**(1), pp. 31–39.

[22] Arruda, E. M., and Boyce, M. C., 1993, “A Three-Dimensional Constitutive Model for the Large Stretch Behavior of Rubber Elastic Materials,” J. Mech. Phys. Solids, **41**(2), pp. 389–412.

[23] Bergström, J. S., and Boyce, M. C., 2000, “Large Strain Time-Dependent Behavior of Filled Elastomers,” Mech. Mater., **32**(11), pp. 627–644.

[24] Mooney, M., 1940, “A Theory of Large Elastic Deformation,” J. Appl. Phys., **11**(9), pp. 582–592.

[25] Rivlin, R., 1948, “Large Elastic Deformations of Isotropic Materials IV. Further Developments of the General Theory,” Philos. Trans. R. Soc. London. Ser. A, Math. Phys. Sci., **241**(835), pp. 379–397.

[26] Kurtz, S. M., Villarraga, M. L., Herr, M. P., Bergström, J. S., Rimnac, C. M., and Edidin, A. A., 2002, “Thermomechanical Behavior of Virgin and Highly Crosslinked Ultra-High Molecular Weight Polyethylene Used in Total Joint Replacements,” Biomaterials, **23**(17), pp. 3681–3697.

Journal of Manufacturing Science and Engineering. Received February 11, 2021;
Accepted manuscript posted May 10, 2021. doi:10.1115/1.4051189

[27] Schmid, S. R., Saha, P. K., Wang, J., and Schmitz, T., 2020, “Developments in Tribology of Manufacturing Processes,” J. Manuf. Sci. Eng., **142**(11), pp. 1–11.

[28] Imado, K., Miura, A., Nagatoshi, M., Kido, Y., Miyagawa, H., and Higaki, H., 2004, “A Study of Contact Temperature Due to Frictional Heating of UHMWPE,” Tribol. Lett., **16**(4), pp. 265–273.

[29] Barceinas-Sanchez, J. D. O., Alvarez-Vera, M., Montoya-Santiyanes, L. A., Dominguez-Lopez, I., and Garcia-Garcia, A. L., 2017, “The Coefficient of Friction of UHMWPE along an Entire Walking Cycle Using a Ball-on-Disc Tribometer under Arthrokinematics and Loading Conditions Prescribed by ISO 14243-3:2014,” J. Mech. Behav. Biomed. Mater., **65**, pp. 274–280.

[30] Agwa, M. A., and Ali, M. N., 2018, “Effective Damage Indicator for Aluminum Alloy (AA6082Zr) Processed by ECAE,” J. Manuf. Sci. Eng. Trans. ASME, **140**(12), pp. 1–10.

[31] Dal, H., and Kaliske, M., 2009, “Bergström-Boyce Model for Nonlinear Finite Rubber Viscoelasticity: Theoretical Aspects and Algorithmic Treatment for the FE Method,” Comput. Mech., **44**(6), pp. 809–823.

[32] Kulkarni, S. S., and Mocko, G. M., 2020, “A Finite Element Simulation Model of Convective Heat-Assisted Single-Point Incremental Forming of Thermoplastics,” Int. J. Adv. Manuf. Technol., **111**(11–12), pp. 3305–3317.

[33] Shahin, A., Barsoum, I., and Islam, M. D., 2020, “Constitutive Model Calibration of the Time and Temperature-Dependent Behavior of High Density Polyethylene,” Polym. Test., **91**(August), p. 106800.

Journal of Manufacturing Science and Engineering. Received February 11, 2021;
Accepted manuscript posted May 10, 2021. doi:10.1115/1.4051189

Figure Captions List

Fig. 1 ECAE schematics. The layers illustrate the nature of the billet deformation during extrusion

Fig. 2 Deformed shape of the polymer billet after the extrusion. Circled is a portion of the billet separated during the extrusion ("dead zone")

Fig. 3 3D FE mesh of the billet (A) undeformed and (B) during the extrusion

Fig. 4 One dimension rheological representation of Bergstrom-Boyce model. μ_A, λ_A^{lock} and κ, μ_B, λ_B^{lock}, τ_{base}, C, m, ($\lambda_A^{lock} = \lambda_B^{lock}$) are the material parameters associated with networks A and B, correspondingly. Explicit expressions for stresses acting on the networks are provided in Appendix A

Fig. 5 One dimensional rheological representation of Three Network Model. μ_A, λ_A^{lock}, κ, $\theta, \hat{\tau}_A$, α, m_A, n, μ_B, μ_{Bf}, $\lambda_B^{lock}, \hat{\tau}_B, m_B$, μ_C, λ_C^{lock}, q, ($\lambda_A^{lock} = \lambda_B^{lock} = \lambda_C^{lock}$) are the material parameters associated with networks A, B and C. Explicit expressions for stresses acting on the networks are provided in Appendix B

Fig. 6 Punch force vs. extrusion time for ECAE of HDPE at 25°C and 60°C. Comparison of the present model with the predictions published in [7]

Fig. 7 Punch force vs. punch displacement for different friction coefficients. The insets illustrate the corresponding stages of the extrusion process

Fig. 8 Deformed shapes using J_2-Plasticity, 2D vs. 3D (μ=0.15)

Journal of Manufacturing Science and Engineering. Received February 11, 2021;
Accepted manuscript posted May 10, 2021. doi:10.1115/1.4051189

Fig. 9	Punch force vs. punch displacement, 2D vs. 3D
Fig. 10	Deformed shape of the billet after the extrusion and extraction
Fig. 11	Punch force vs. punch displacement for different constitutive models
Fig. 12	Maximum shear strain distribution as predicted by the J_2, BB and TNM models. Simulations are performed for extrusion at 20ºC
Fig. 13	Mitre-fillet-like insert schematics. Dimensions are in millimeters
Fig. 14	Comparison of the predictions by a model with the triangular insert and without it. (A) Deformed shapes and (B) punch force – displacement curves. Red circle on the experimental deformed shape indicates the area of severe local plastic deformation
Fig. 15	Maximum shear strain predicted by the model (A) without a triangular insert and (B) including a triangular insert
Fig. 16	Punch force - displacement curves for different temperatures

Journal of Manufacturing Science and Engineering. Received February 11, 2021;
Accepted manuscript posted May 10, 2021. doi:10.1115/1.4051189

Table Caption List

Table 1 J_2-Plasticity model parameters for HDPE

Journal of Manufacturing Science and Engineering. Received February 11, 2021;
Accepted manuscript posted May 10, 2021. doi:10.1115/1.4051189

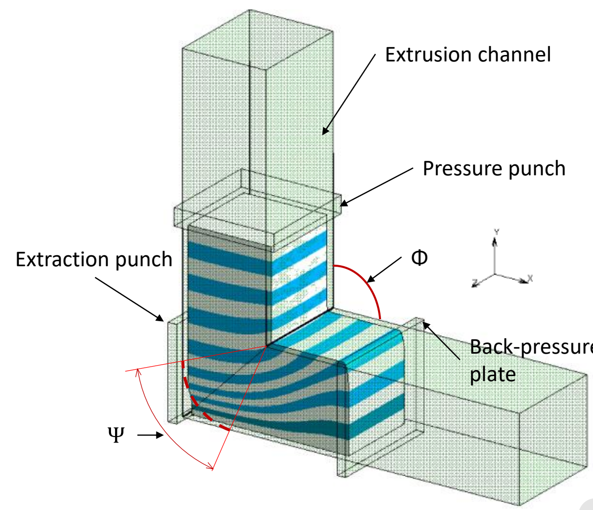

575

576 Fig. 1 ECAE schematics. The layers illustrate the nature of the billet deformation during

577 extrusion

578

Journal of Manufacturing Science and Engineering. Received February 11, 2021;
Accepted manuscript posted May 10, 2021. doi:10.1115/1.4051189

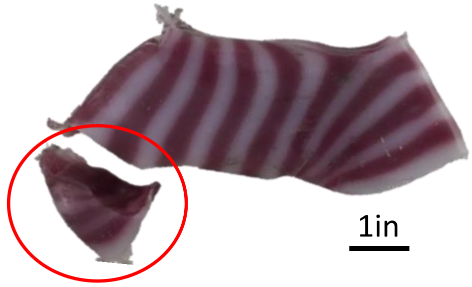

Fig. 2 Deformed shape of the polymer billet after the extrusion. Circled is a portion of the billet separated during the extrusion ("dead zone")

Journal of Manufacturing Science and Engineering. Received February 11, 2021;
Accepted manuscript posted May 10, 2021. doi:10.1115/1.4051189

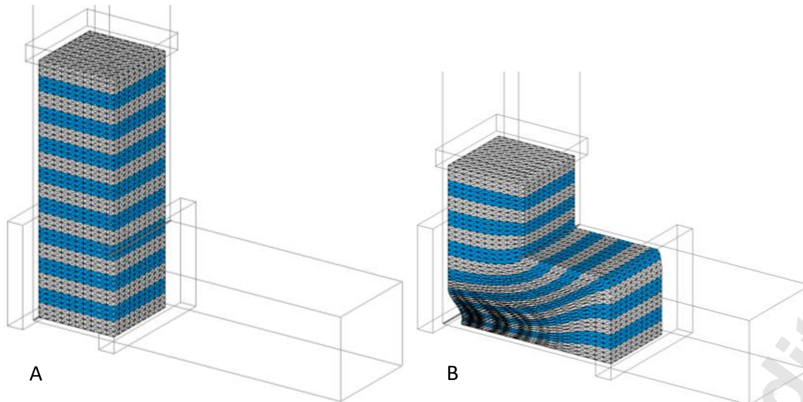

Fig. 3 3D FE mesh of the billet (A) undeformed and (B) during the extrusion

Journal of Manufacturing Science and Engineering. Received February 11, 2021;
Accepted manuscript posted May 10, 2021. doi:10.1115/1.4051189

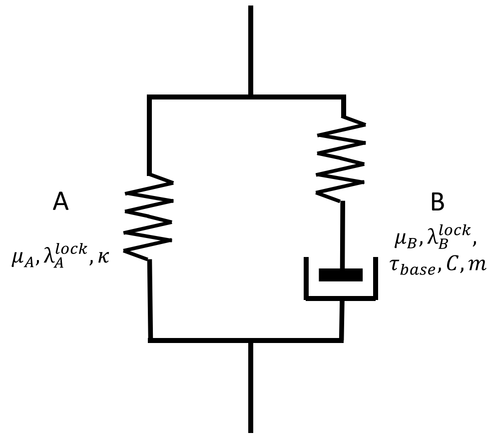

586

587 Fig. 4 One dimension rheological representation of Bergstrom-Boyce model.

588 μ_A, λ_A^{lock} and κ, μ_B, λ_B^{lock}, τ_{base}, C, m, ($\lambda_A^{lock} = \lambda_B^{lock}$) are the material parameters associated

589 with networks A and B, correspondingly. Explicit expressions for stresses acting on the networks

590 are provided in Appendix A

591

Journal of Manufacturing Science and Engineering. Received February 11, 2021;
Accepted manuscript posted May 10, 2021. doi:10.1115/1.4051189

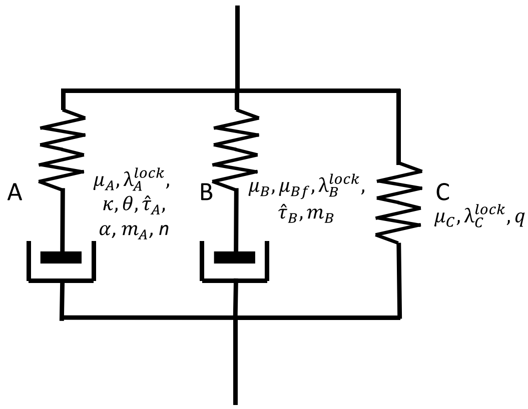

592

593 Fig. 5 One dimensional rheological representation of Three Network Model.

594 μ_A, λ_A^{lock}, κ, $\theta, \hat{\tau}_A$, $\alpha, m_A, n, \mu_B, \mu_{Bf}$, $\lambda_B^{lock}, \hat{\tau}_B, m_B$, μ_C, λ_C^{lock}, q, $(\lambda_A^{lock} = \lambda_B^{lock} = \lambda_C^{lock})$ are the
595 material parameters associated with networks A, B and C. Explicit expressions for stresses acting
596 on the networks are provided in Appendix B

597

Journal of Manufacturing Science and Engineering. Received February 11, 2021;
Accepted manuscript posted May 10, 2021. doi:10.1115/1.4051189

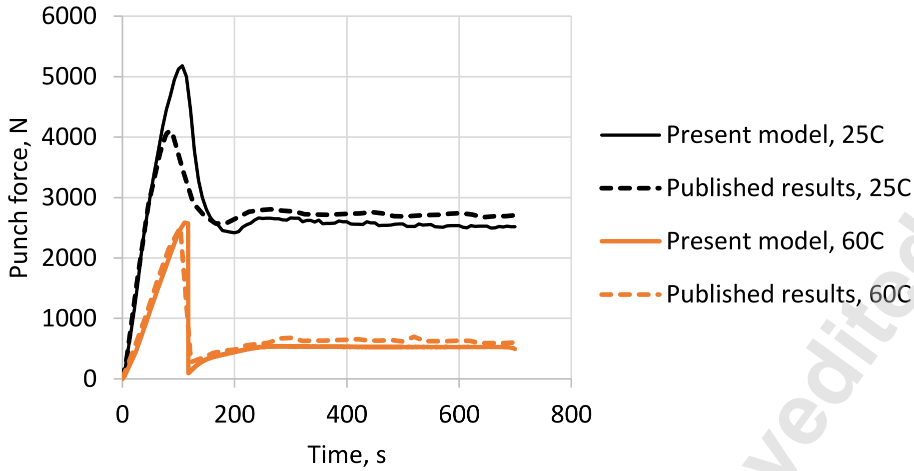

Fig. 6 Punch force vs. extrusion time for ECAE of HDPE at 25°C and 60°C. Comparison of the present model with the predictions published in [7]

Journal of Manufacturing Science and Engineering. Received February 11, 2021;
Accepted manuscript posted May 10, 2021. doi:10.1115/1.4051189

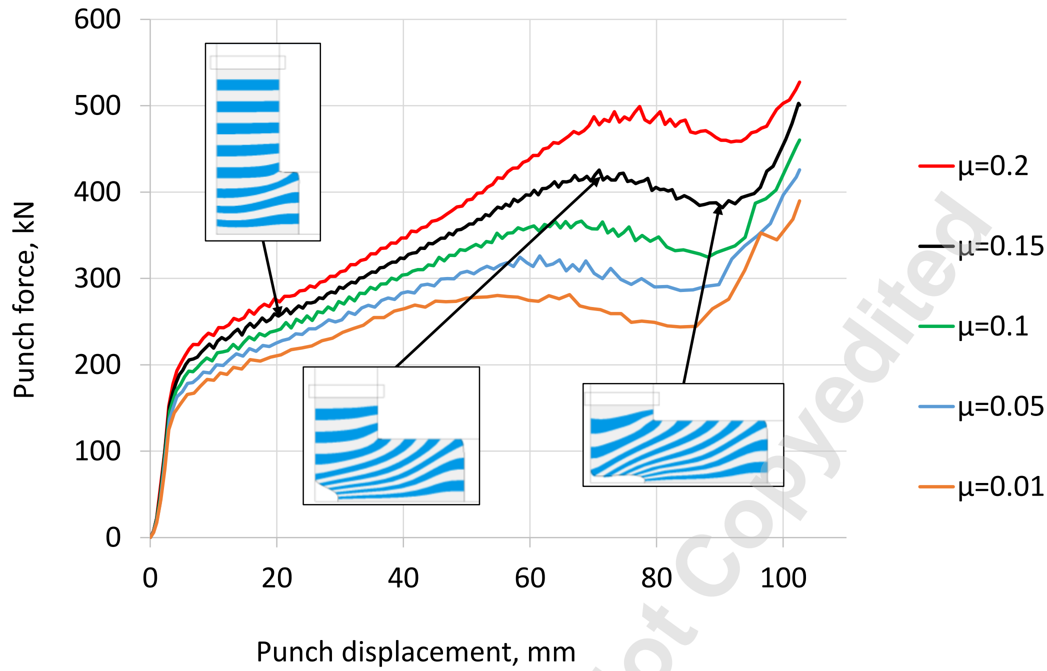

602
603 Fig. 7 Punch force vs. punch displacement for different friction coefficients. The insets
604 illustrate the corresponding stages of the extrusion process
605

Journal of Manufacturing Science and Engineering. Received February 11, 2021;
Accepted manuscript posted May 10, 2021. doi:10.1115/1.4051189

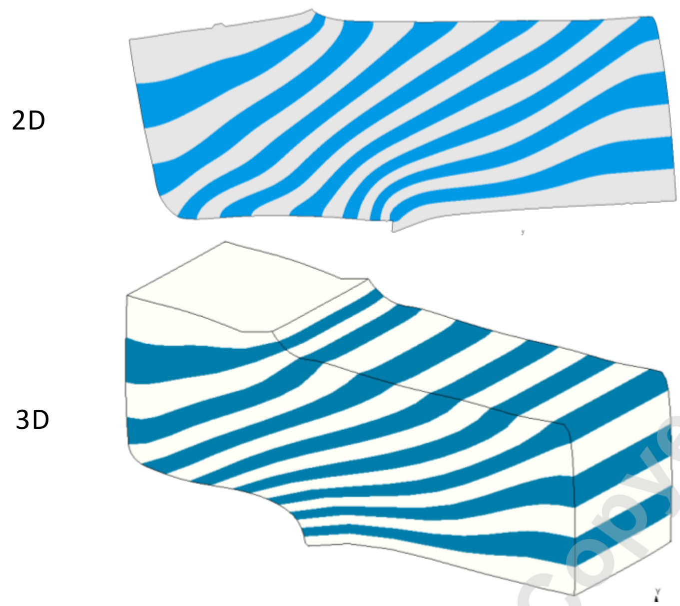

Fig. 8 Deformed shapes using J_2-Plasticity, 2D vs. 3D (μ=0.15)

Journal of Manufacturing Science and Engineering. Received February 11, 2021;
Accepted manuscript posted May 10, 2021. doi:10.1115/1.4051189

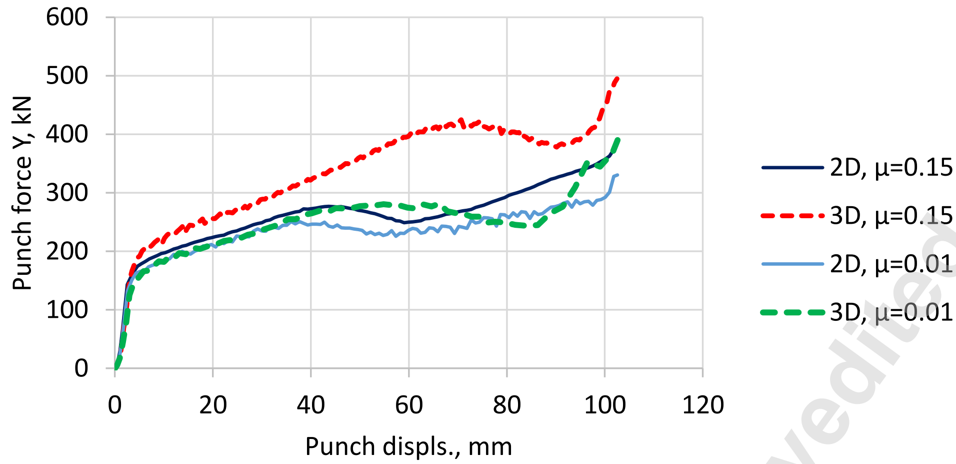

609

610 Fig. 9 Punch force vs. punch displacement, 2D vs. 3D

611

Journal of Manufacturing Science and Engineering. Received February 11, 2021;
Accepted manuscript posted May 10, 2021. doi:10.1115/1.4051189

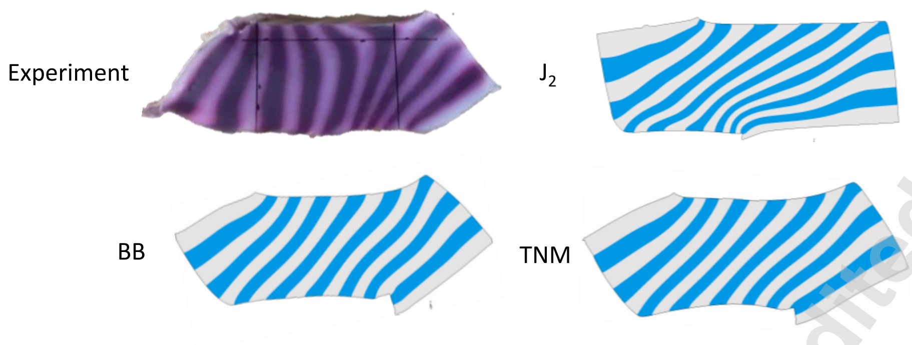

612

613 Fig. 10 Deformed shape of the billet after the extrusion and extraction

614

Journal of Manufacturing Science and Engineering. Received February 11, 2021;
Accepted manuscript posted May 10, 2021. doi:10.1115/1.4051189

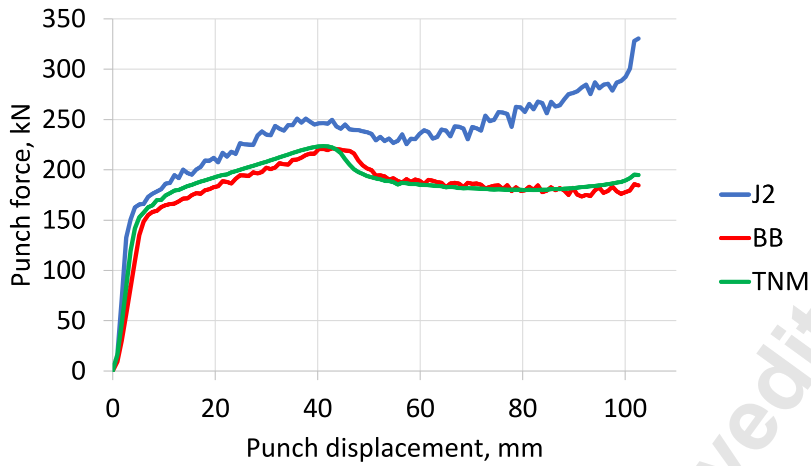

615

616 Fig. 11 Punch force vs. punch displacement for different constitutive models

617

Journal of Manufacturing Science and Engineering. Received February 11, 2021;
Accepted manuscript posted May 10, 2021. doi:10.1115/1.4051189

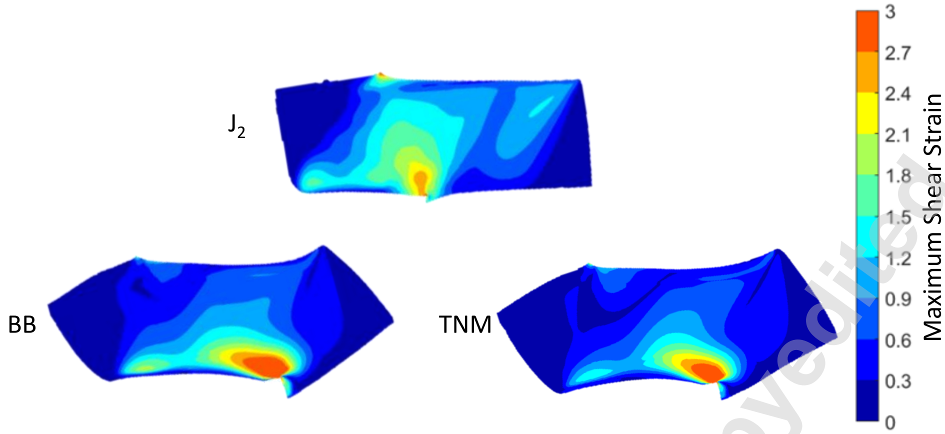

Fig. 12 Maximum shear strain distribution as predicted by the J_2, BB and TNM models. Simulations are performed for extrusion at 20ºC

Journal of Manufacturing Science and Engineering. Received February 11, 2021;
Accepted manuscript posted May 10, 2021. doi:10.1115/1.4051189

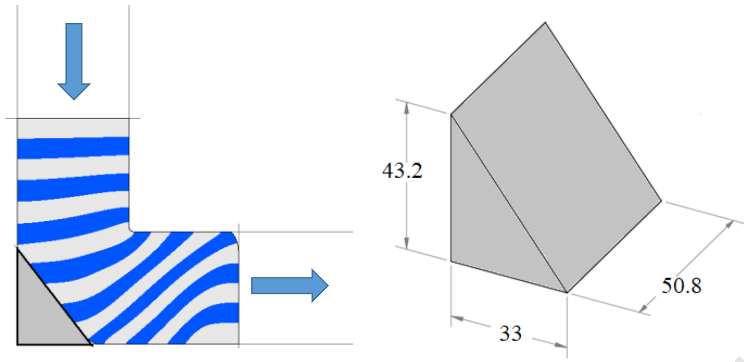

623

624 Fig. 13 Mitre-fillet-like insert schematics. Dimensions are in millimeters

625

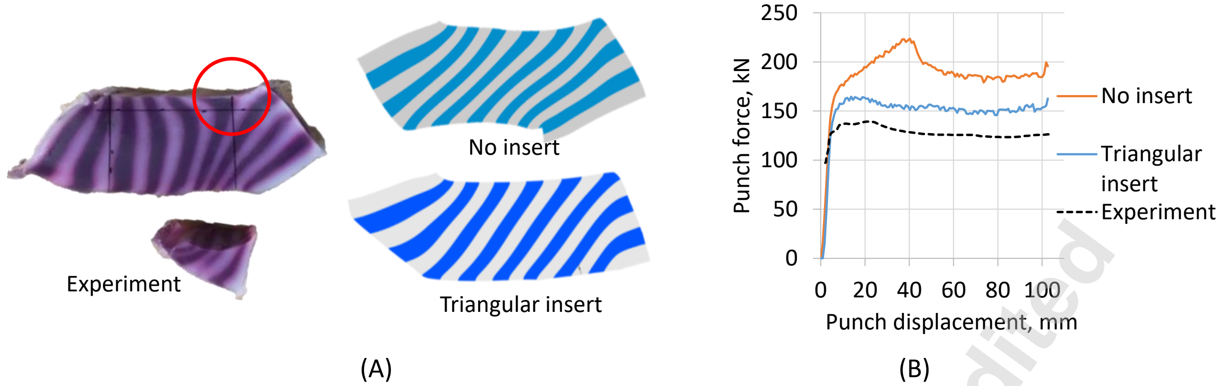

Fig. 14 Comparison of the predictions by a model with the triangular insert and without it. (A) Deformed shapes and (B) punch force – displacement curves. Red circle on the experimental deformed shape indicates the area of severe local plastic deformation

Journal of Manufacturing Science and Engineering. Received February 11, 2021;
Accepted manuscript posted May 10, 2021. doi:10.1115/1.4051189

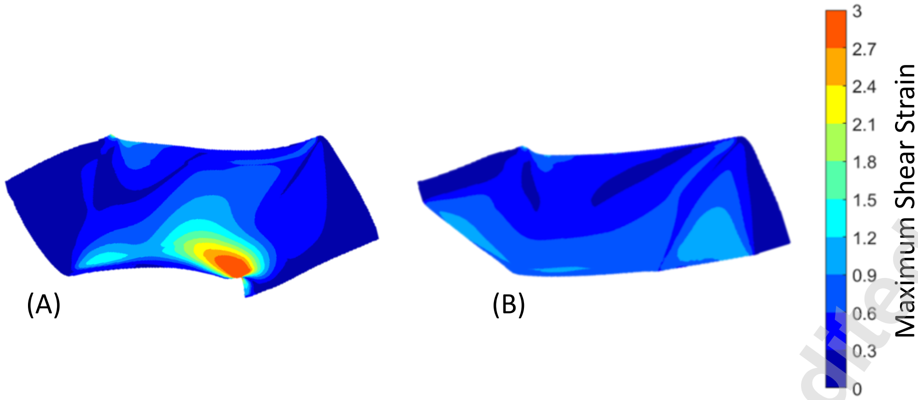

Fig. 15 Maximum shear strain predicted by the model (A) without a triangular insert and (B) including a triangular insert

Journal of Manufacturing Science and Engineering. Received February 11, 2021;
Accepted manuscript posted May 10, 2021. doi:10.1115/1.4051189

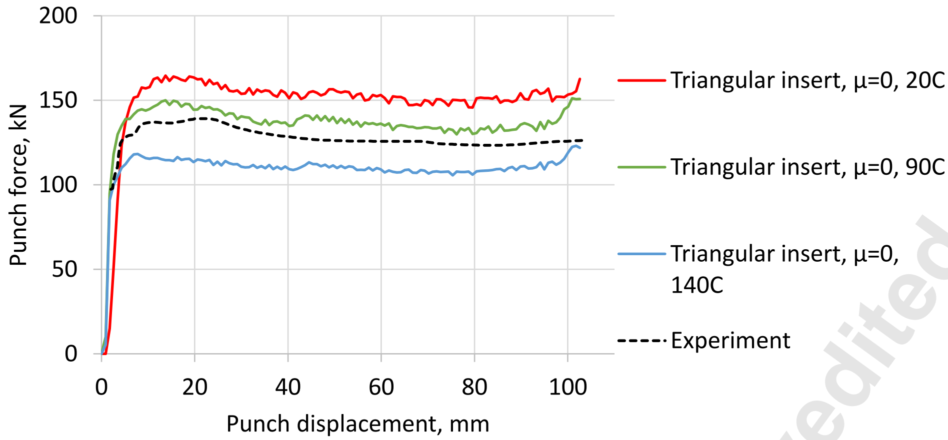

635

636 Fig. 16 Punch force - displacement curves for different temperatures

637

Journal of Manufacturing Science and Engineering. Received February 11, 2021;
Accepted manuscript posted May 10, 2021. doi:10.1115/1.4051189

638 Table I: J_2-Plasticity model parameters for HDPE

T=25°C		T=60°C	
E, MPa	500	E, MPa	150
ν	0.38	ν	0.38
ε_p	$\bar{\sigma}_Y$, MPa	ε_p	$\bar{\sigma}_Y$, MPa
0	10.0	0	3.6
0.0027	16.4	0.0184	9.1
0.0807	25.1	0.0771	15.9
0.1614	31.5	0.1124	19.1
0.2595	36.0	0.1537	22.1
0.2133	39.4	0.1905	24.3
0.3306	44.8	0.2299	26.6

639